

## Torsional Fretting Corrosion Behaviors of the CoCrMo/Ti6Al4V Couple

Songquan Wang<sup>1,\*</sup>, Dekun Zhang<sup>2,\*</sup>, Meng Sun<sup>1</sup>, Ningning Hu<sup>1</sup>

<sup>1</sup> School of Mechatronic Engineering, JiangSu Normal University, 101# Shanghai Road, Xuzhou 221116, China

<sup>2</sup> School of Materials Science and Engineering, China University of Mining and Technology, 1# University Road, Xuzhou 221116, China

\*E-mail: [wbplsz@outlook.com](mailto:wbplsz@outlook.com), [dkzhang@cumt.edu.cn](mailto:dkzhang@cumt.edu.cn)

Received: 5 April 2018 / Accepted: 10 May 2018 / Published: 5 June 2018

---

There are different forms of fretting corrosion on the fitting surface of hip prosthesis head and neck, which have an impact on the service life of the implant. In this paper, the torsional fretting corrosion experiment of CoCrMo alloy and Ti6Al4V alloy in FBS solution was simulated by simulating the head-neck taper contact mode of the hip joint. The effects of angular displacement amplitude and contact load on the wear mechanism and electrochemical corrosion properties of prosthesis materials were discussed. The results showed that the value of friction torque first increased and then tended to be stable at the taper contact interface of CoCrMo head and Ti6Al4V neck under the condition of small normal load. However, the friction torque was stable at early stage with no significant increase under larger loads. After friction, the corrosion potential of CoCrMo alloy was significantly negative and the current of the anode region was obviously increased, which showed that the corrosion tendency of materials increased. According to the results of the electrochemical corrosion test, the impedance of CoCrMo alloy after friction decreased significantly, as well as the polarization resistance. When the angle displacement amplitude  $\theta=2^\circ$ , obvious slip band could be found on the sample surface, which was badly worn and corroded under small normal load. Under larger normal load, a large number of scratches along the twisting direction appeared on the worn surface, accompanied by peeling and corrosion of the material. The relative movement of the sample surface was mainly based on partial slip.

---

**Keywords:** Torsional fretting corrosion, contact surface, CoCrMo/Ti6Al4V

### 1. INTRODUCTION

Total hip replacement (THR) is now the most effective way to treat the various pathological changes of hip joint disease. However, the service life of current hip prosthesis used in the body is not

high, which is generally maintained for about 10-15 years [1]. Among them, the aseptic loosening of the prosthesis is the most important form of failure. A lot of research shows that the prosthesis interface friction and wear is the most important cause of aseptic loosening, and the fretting on the contact surfaces of prosthesis is one of the most important forms [2-4]. At the same time, fretting corrosion occurs under the synergistic effect of human body fluid erosion, which further affects the service life of prosthesis.

Researchers have conducted extensive studies on the fretting corrosion behavior of artificial hip prostheses [5-10]. Kim K [5-6] carried out the fretting corrosion test of stainless steel (316L) and poly (methyl methacrylate) couple used for total hip prosthesis in Ringer's solution, and analysed the energy dissipation of fretting corrosion and the friction coefficient evolution between materials. Geringer J [7] described how to use the electrochemical impedance spectroscopy (EIS) to study the fretting corrosion behavior of hip prosthesis, and studied the influence of ionic strength and a model protein, albumin, on passive layer behavior. Liu [8] discussed the effect of simulated inflammatory conditions and pH on fretting corrosion of CoCrMo alloy surfaces by the friction test of pin and disk. Royhman [9] studied the fretting corrosion behavior of CoCrMo-Ti6Al4V couple under different applied potential. And Santos [10] carried out in-depth analysis respectively on the surface damage and residues of different friction pairs released during in vitro fretting corrosion tests, and the results showed that fretting corrosion in the inner surface of the head and in the head-taper interface was observed in the stainless steel/stainless steel prostheses, which also resulted in particulate debris and corrosion products. Obviously, an increase number of early failure of hip prosthesis has been attributed to fretting-corrosion at modular interfaces.

As the most common hip prosthesis, combined artificial hip prosthesis is widely used. Under the periodic load of human body movement and the corrosion of synovial fluid, fretting corrosion occurs on the head-neck fitting surface of combined artificial hip joint prosthesis the action of synovial fluid. Long-term effects may cause the failure of implants or even endanger human health. CoCrMo and Ti6Al4V alloys are widely used because of their good biocompatibility in the material selection of combined artificial hip prostheses. CoCrMo alloy has excellent wear resistance, but the proportion is large, while Ti6Al4V has a high specific strength, low modulus of elasticity and fatigue resistance. Therefore, CoCrMo alloy is commonly used as a joint head, and Ti6Al4V alloy is used as an articular handle [11]. According to the research of J.S. Kawalec [12] and M.Viceconti [13], the two kinds of alloys couple is very sensitive to fretting corrosion.

In recent years, the fretting corrosion behavior of contact surface between CoCrMo alloy and Ti6Al4V alloy has also been extensively studied [9, 14-16]. V Swaminathan [14, 15] established a fretting corrosion test system and presented an in-depth theoretical fretting corrosion model that incorporated both the mechanical and the electrochemical aspects of fretting corrosion. The fretting corrosion model was verified by the pin-disk fretting corrosion test of three groups of different pairs (Ti6Al4V/Ti6Al4V, CoCrMo/Ti6Al4V, and CoCrMo/CoCrMo). The results showed that fretting corrosion was affected by material couples, normal load, potential, frequency and the motion conditions at the interface. In addition, CoCrMo/Ti6Al4V couple reported the lowest fretting currents compared to CoCrMo/CoCrMo and Ti6Al4V/CoCrMo couples.

The above research detailed the fretting corrosion behavior of the CoCrMo/Ti6Al4V couple, but most of the experimental methods still stayed in the pin-disk or disk-disk contact mode. And there were few fretting corrosion studies directly on the contact surface between CoCrMo head and Ti6Al4V neck. Although some research [17-19] studied the friction behavior on the head-neck interface by the finite element simulation, the finite element method could not analyze the behavior of fretting corrosion. In this paper, CoCrMo alloy and Ti6Al4V alloy were used as the research object to simulate the contact pattern of the head-neck of artificial hip joint, and the torsional fretting corrosion experiment was conducted between two materials in FBS solution. Based on the in-depth analysis of  $T$ - $\theta$  curve, friction torque time-varying curve and EIS, the operating characteristics and damage mechanism of torsional fretting corrosion between CoCrMo head and Ti6Al4V neck under different experimental conditions were revealed.

## 2. EXPERIMENTAL

### 2.1 Materials

In this study, fetal bovine serum (FBS, 25% volume of calf serum) was used as the corrosive medium. Meanwhile, CoCrMo alloy and Ti6Al4V alloy were selected as the research object. The chemical composition and related physical mechanical properties of both alloys were shown in Table 1 and 2 [18, 20].

**Table 1.** Chemical composition of CoCrMo and Ti6Al4V (Mass percentage)

CoCrMo	Co	Cr	Mo	Ni	Fe	Mn	Si	C	N
	63.25	28.10	5.90	0.88	0.65	0.63	0.22	0.25	0.12
Ti6Al4V	Ti	Al	V	Fe	C	O	N	H	
	89.729	6.05	3.95	0.11	0.014	0.14	0.006	0.001	

**Table 2.** Physical mechanical properties of Ti6Al4V and CoCrMo

Materials	Tensile strength (MPa)	Yield strength (MPa)	Elongation ratio (%)	Elastic modulus (GPa)	Poisson ratio	Hardness (HV)
Ti6Al4V	950	860	12	110	0.3	348
CoCrMo	970	660	18	200	0.3	321

The head-neck model was simplified referenced to the geometric parameters of the head and neck of prosthesis [18]. The CoCrMo alloy ring with a tapered hole was selected as the prosthesis

head, and the Ti6Al4V alloy was selected as the prosthesis neck. The taper of the joint surface was 5 °. The motion pattern of the samples was shown in Fig. 1.

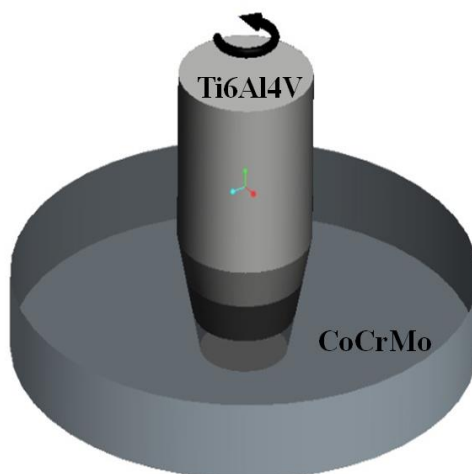


**Figure 1.** Sample schematic of torsional fretting test

## 2.2 Methods

The homemade experimental device based on the UMT-3 friction wear testing machine was used for this torsional fretting corrosion test, which was introduced in detail in reference [18, 20]. The variation curve of friction torque ( $T$ ) - angular displacement amplitude ( $\theta$ ) at different cycle times ( $N$ ) was obtained by Matlab 7.0. The change trend of the friction torque with the cycle was obtained by dealing with the relationship between the friction torque and the amplitude of the angular displacement with the change of the cycle. Table 3 showed the experimental parameters of the torsional fretting corrosion test. After the test, the macroscopic morphology and micromorphology of the contact surface of Ti6Al4V specimen were observed by optical microscope and scanning electron microscope (SEM) respectively.

**Table 3.** Parameters of torsional fretting corrosion test

Test parameters	Value
Normal load/ $F_n$	5 N, 10 N
Fretting angular displacement/ $\theta$	1.5 °, 2 °
Fretting frequency/ $f$	1 Hz
Cyclic number/ $N$	4800

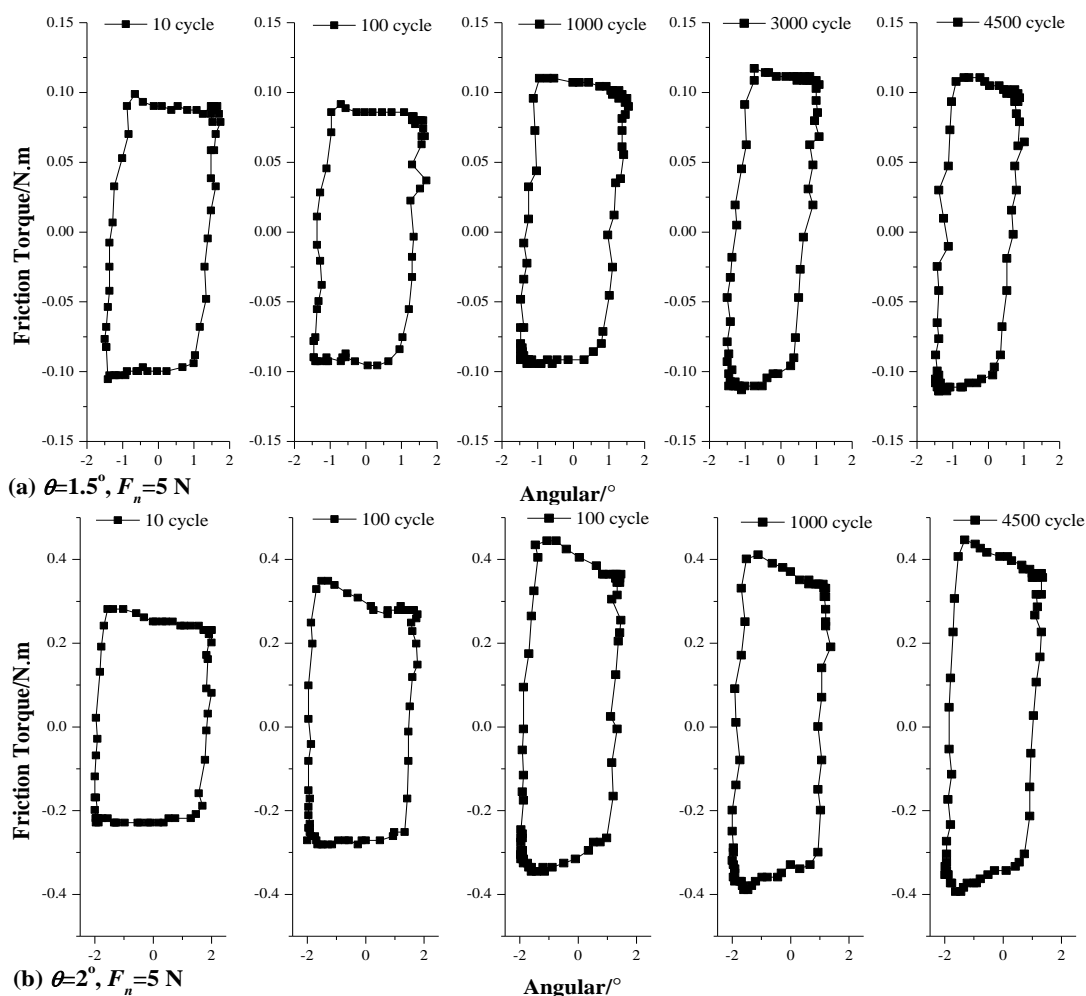
The electrochemical performance of CoCrMo alloy before and after friction was measured by the electrochemical workstation of CS type. The Ag/AgCl reference electrode was selected as the reference electrode, the platinum electrode (10×10×0.1 mm, purity 99.99%) was used as the counter electrode, and the CoCrMo alloy was the working electrode. When measuring the polarization curve,

the potential scan range had an open circuit potential of electrodes (relative to the Ag-AgCl electrodes)  $\pm 500$  mV and a scan rate of 1 mV/s. The EIS test was carried out with a frequency of  $10^5 - 10^2$  Hz and an AC signal amplitude of 10 mV.

### 3. RESULTS

#### 3.1 T- $\theta$ Curve

Fig. 4 showed the friction torque ( $T$ ) - angular displacement amplitude ( $\theta$ ) curve of the contact surface of CoCrMo head and Ti6Al4V neck under different cycle times in FBS. When  $F_n=5$  N and  $\theta=1.5^\circ$ , the  $T$ - $\theta$  curve presented a parallelogram shape from the initial cycle to the end of the cycle, and the friction torque increased gradually. When the  $\theta$  increased to  $2^\circ$ , the  $T$ - $\theta$  curve presented a parallelogram shape from the beginning of the experiment to the 100 cycle. With the increase of the cycle, the  $T$ - $\theta$  curve was gradually transformed into a ladder shape, which showed that the tangential torsion and normal relative motion of contact surface occurred simultaneously. The contact surface of the materials was run in the completely slip state during the whole torsional fretting process.



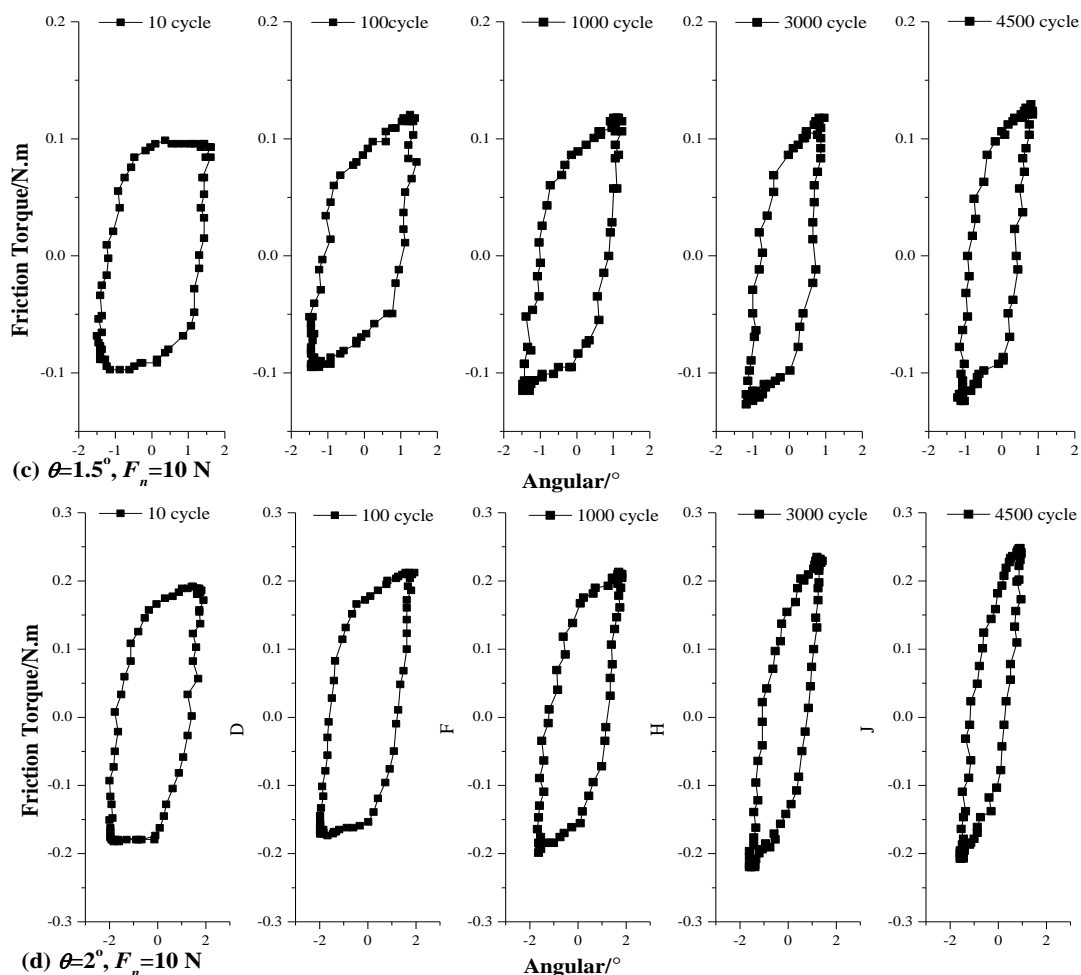


**Figure 4.**  $T$ - $\theta$  curves of torsional fretting under different cycles and different normal load in FBS, (a)  $\theta=1.5^\circ$ ,  $F_n=5$  N, (b)  $\theta=2^\circ$ ,  $F_n=5$  N, (c)  $\theta=1.5^\circ$ ,  $F_n=10$  N, (d)  $\theta=2^\circ$ ,  $F_n=10$  N

When  $F_n=10$  N, the large normal load could cause large frictional force on the contact surface. Under small angle, the relative movement between material interfaces was mainly controlled by elastic-plastic deformation [20]. The  $T$  increased gradually with the increase of  $\theta$ . In the process of torsion, the  $T$ - $\theta$  curve presented an ellipse shape in the case of less cycle. Under the condition of large  $\theta$ , the relative motion of material needed to overcome the great friction, which caused that the complete slip state was hard to be formed. At this time, the torsion was mainly run in the partial slip state.

### 3.2 Polarization curve

Fig. 5 showed the dynamic polarization curves of CoCrMo alloys before and after friction in FBS. It could be seen from the graph that the polarization curve of the sample after friction (in the case of  $F_n=5$  N and  $\theta=2^\circ$ ) had a obvious negative shift. The self corrosion potential was -151 mV before friction and reduced to -346 MV after friction, which showed that the tendency of corrosion increased significantly [9]. And the self corrosion current rose from  $2.042E-7$  Amp/cm<sup>2</sup> before friction to

7.996E-7 Amp/cm<sup>2</sup>, which increased nearly 3 times (as shown in Table 4). All these indicated that the uniformity of surface was damaged by friction, which caused the different thickness and density of surface film of the wear area and non wear area in FBS. There was even obvious potential difference in the local area, which formed a local galvanic corrosion reaction and then decreased the corrosion resistance. In the anode region, the anode current of the specimen after friction increased with the increase of potential. The anode current of the specimen before friction appeared a platform when the anode potential reached 128 MV. And the current did not change obviously with the increase of potential, which showed that the CoCrMo alloy was in the passivation state in this stage [21]. In addition, the anode current of the specimen after friction was larger than that before friction, and there was no obvious passivation zone in the anode region.

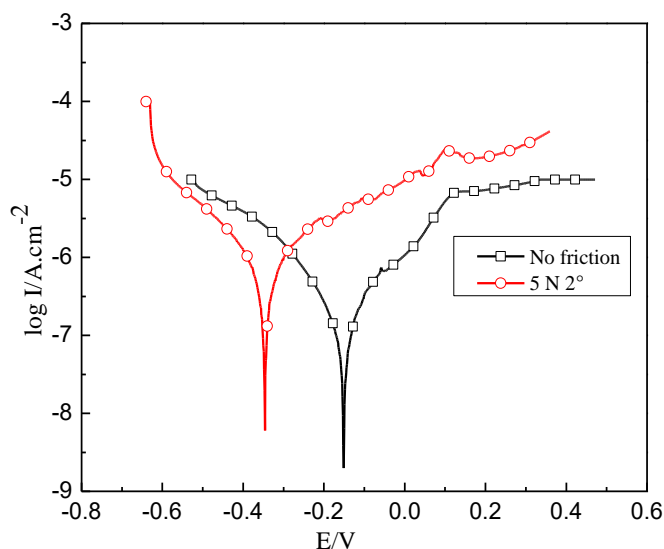


**Figure 5.** Potentiodynamic polarization curves of CoCrMo alloys before and after friction ( $\theta=2^\circ$ ,  $F_n=5\text{ N}$ ) in FBS

**Table 4.** Parameters of potentiodynamic polarization curves of CoCrMo alloys before and after friction in FBS

	Without friction	$F_n=5\text{N}, \theta=2^\circ$
$I_{corr}$ (Amp/cm <sup>2</sup> )	2.042E-7	7.996E-7
$E_{corr}$ (V)	-0.346	-0.151

### 3.3 Electrochemical impedance spectroscopy (EIS)

Fig. 6 showed the Nyquist plots and Bode plots of CoCrMo alloys under different normal load and different angular displacement amplitude. The symbols represented the measured values, and the lines represented the fitting values. All the Nyquist plots presented a single capacitive arc feature. The radius of capacitive arc was larger under small angular displacement amplitude ( $\theta=1.5^\circ$ ), which showed that the surface of sample could maintain good corrosion resistance. This was mainly due to

the fact that the friction of surface was not very intense and the damage to the surface uniformity was not very serious under the condition of small  $\theta$ . However, the impedance decreased obviously with the increase of  $\theta$ . It could be seen from Fig. 6b that the width of the phase angle peak was narrowed and the peak value decreased with the increase of the angular displacement amplitude. In the case of the same normal load, there was a lot of plastic deformation and rough peak produced on the surface of CoCrMo alloy under large  $\theta$ , which caused the damage of surface passivation film and then decreased the corrosion resistance of the surface. However, different normal loads had little influence on the variation of EIS with the variation of angular displacement amplitude.

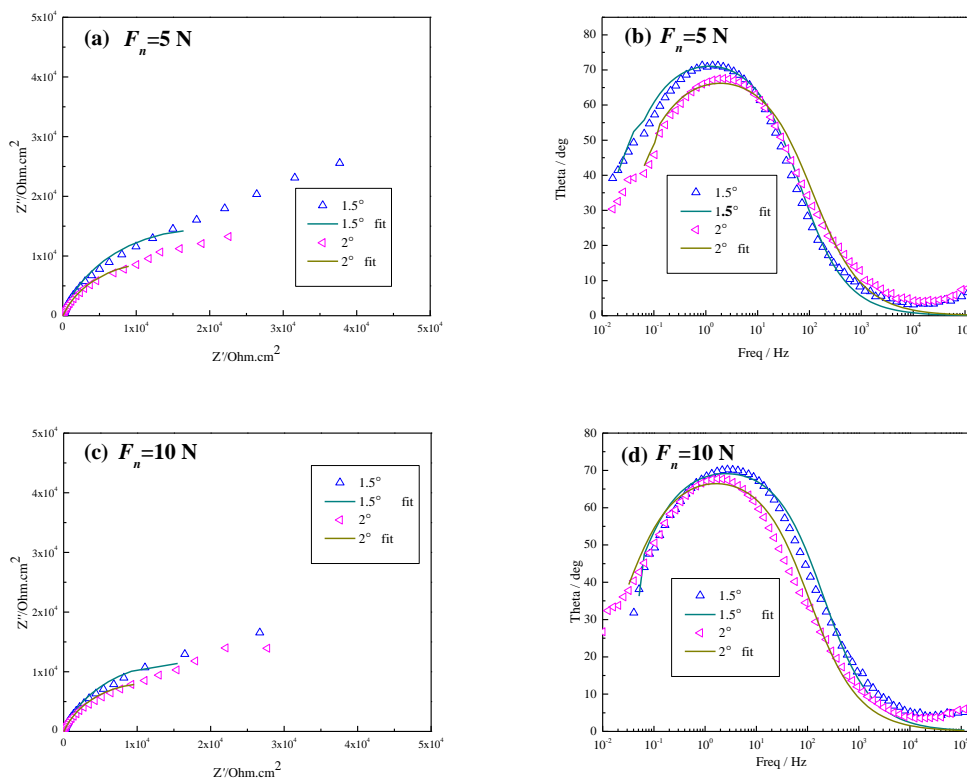


**Figure 6.** Nyquist plots and Bode plots of CoCrMo alloys under different normal load and different angular displacement amplitude in FBS, (a) Nyquist plots,  $F_n = 5\text{ N}$ , (b) Bode plots,  $F_n = 5\text{ N}$ , (c) Nyquist plots,  $F_n = 10\text{ N}$ , (d) Bode plots,  $F_n = 10\text{ N}$

#### 4. DISCUSSION

According to the results of the  $T-\theta$  curve, it was found that the  $T-\theta$  curve changed from a parallelogram shape to an ellipse ship when the load was constant under small  $\theta$  condition, which showed that the friction process of contact surface changed from the complete slip state to the partial slip state [22, 23]. The friction process of contact surface was run in the complete slip state under the condition of small normal load and large  $\theta$ . Meanwhile, the friction process of contact surface was run in the partial slip state under the condition of large normal load and large  $\theta$  during the late stage of test, which was caused by the difficult relative slip between the materials. This result was also different from the result of the torsional fretting test between CoCrMo ball and Ti6Al4V disk reported by Wang

[24], which showed that the motion pattern had a great influence on the friction process of contact surface. Fig. 7 showed the variation of the torsional fretting friction torque on the contact surface of CoCrMo head and Ti6Al4V neck with the increase of cycles under the condition of different  $\theta$  and different normal load in FBS, which was obtained by the analysis of the  $T-\theta$  curve. It could be seen from the curve that the friction torque rose gradually and tended to be stable under the condition of small normal load. The relative displacement between the contact surfaces increased with the increase of  $\theta$ , which caused that the torsional fretting was run in the sliding state. In the late stage of fretting, the friction torque was relatively stable, which was because the friction was in a dynamic balance for the lubrication of the abrasive (the third body) caused by friction and the bovine serum. In the case of large normal load, the friction torque was slightly rising, and tended to be stable after a few cycles. In addition, the value of friction torque was larger under large  $\theta$ , which was due to the need to overcome the rough peak caused by more machining in the process of torsional fretting friction.

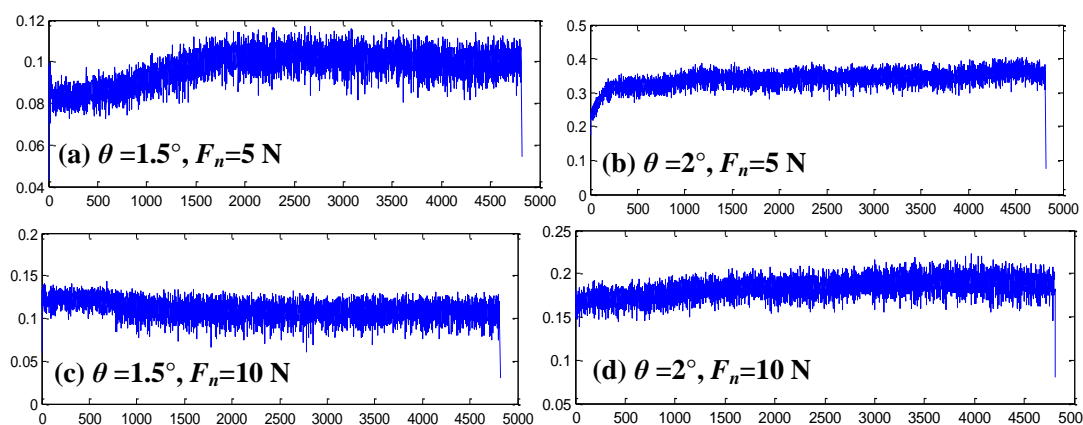


**Figure 7.** Friction torque change with different time in FBS (N•m), (a)  $\theta=1.5^\circ$ ,  $F_n=5$  N, (b)  $\theta=2^\circ$ ,  $F_n=5$  N, (c)  $\theta=1.5^\circ$ ,  $F_n=10$  N, (d)  $\theta=2^\circ$ ,  $F_n=10$  N

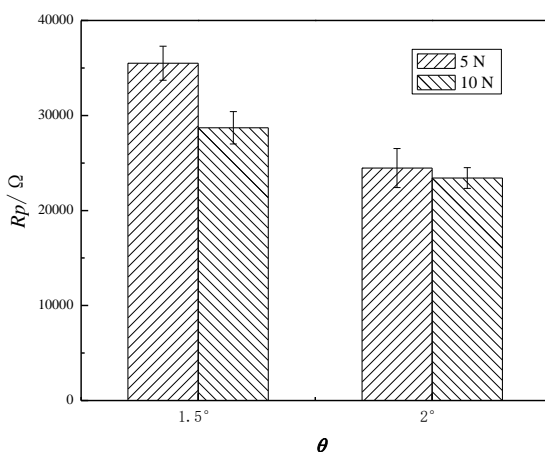


**Figure 8.** Polarization resistance of CoCrMo alloy under different angular displacement amplitude in FBS

As shown in Fig. 8, the polarization resistance of CoCrMo alloy under the condition of different  $\theta$  in FBS was obtained by the analysis of the EIS. When  $\theta=1.5^\circ$  and  $F_n=5$  N, the polarization resistance of CoCrMo alloy was the largest, which reached 35498  $\Omega$ . And when  $\theta=2^\circ$  and  $F_n=10$  N, the polarization resistance of CoCrMo alloy was the smallest, which reached 23422  $\Omega$ . Under the same  $F_n$ , the polarization resistance of CoCrMo alloy decreased with the increase of  $\theta$ . Meanwhile, Under the same  $\theta$ , the polarization resistance of CoCrMo alloy also decreased with the increase of  $F_n$ . With the increase of  $\theta$ , the uniformity of the surface was damaged by the intense friction between the contact surfaces. The inhomogeneous passivation film led to the local potential difference, which induced the galvanic corrosion reaction and thus decreased the polarization resistance. Moreover, the larger the  $\theta$  was, the lower the polarization resistance was. In addition, the influence of the  $\theta$  was larger than that of the normal load on the polarization resistance.

Fig. 9 showed the optical morphology of Ti6Al4V wear surface under different working conditions in FBS. The roughness of surface was larger due to the mechanical processing of the sample. And the color of surface was dark because the surface was covered with an oxide film (as shown in Fig. 9a). When  $\theta=2^\circ$  and  $F_n=5$  N (as shown in Fig. 9b), there was an obvious slip band on the surface of sample. The wear in the slip band accompanied by a large amount of debris accumulation, material exfoliation and corrosion craters was serious. Meanwhile, there were scratches with the same direction of wear in other areas, which showed that the contact surface was run in complete slip state. This was also in agreement with the results of the  $T$ - $\theta$  curve. When  $\theta=2^\circ$  and  $F_n=10$  N (as shown in Fig. 9c), a large number of scratches along the torsional direction appeared on the worn surface. It could be seen that the increase of normal load would aggravate the damage of wear surface.

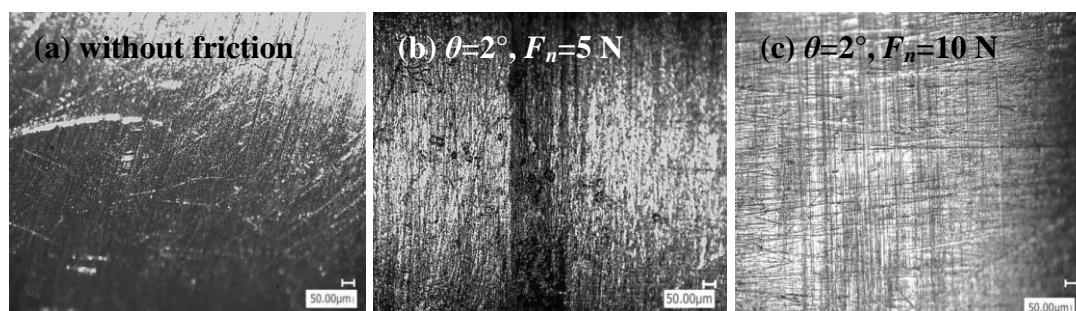


**Figure 9.** Optical morphology of Ti6Al4V wear surface in FBS, (a) without friction, (b)  $\theta=2^\circ$ ,  $F_n=5$  N, (c)  $\theta=2^\circ$ ,  $F_n=10$  N

In order to further study the mechanism of interface wear, the micromorphology of Ti6Al4V wear surface in FBS was shown in Fig. 10. Compared with Fig. 9b, it was found that the number and width of furrow increased with the increase of angular displacement amplitude, while there was no obvious sign of corrosion. Compared with Fig. 10a, the degree of abrasive wear increased gradually with the increase of normal load as shown in Fig. 10b. In addition, due to severe wear, large particles were involved in the next step of friction and wear, resulting in the appearance of deep scratches.

Under this condition, the joint effects of abrasive wear, adhesive wear and corrosion wear aggravated the damage of wear surface [25, 26].

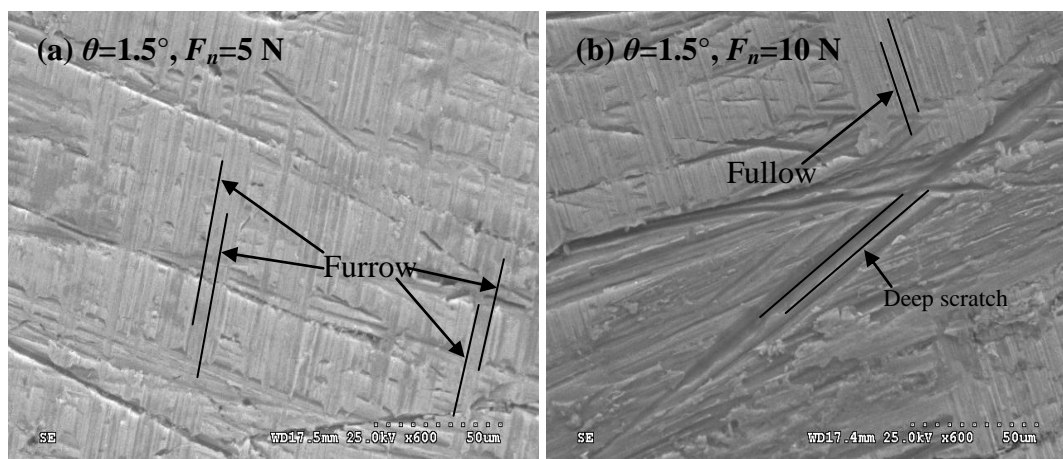


**Figure 10.** SEM of Ti6Al4V wear surface in FBS, (a)  $\theta=1.5^\circ$ ,  $F_n=5$  N, (b)  $\theta=1.5^\circ$ ,  $F_n=10$  N

## 5. CONCLUSION

According to the analysis of  $T-\theta$  curves, it was found that the contact surface was always run in the complete slip state under small load condition ( $F_n=5$  N). Meanwhile, the contact surface was run in the partial slip state under large load condition ( $F_n=10$  N) during the late stage of test. The results of the electrochemical test showed that the angular displacement amplitude had a more significant effect on the electrochemical corrosion resistance of the worn surface of CoCrMo alloy compared with the normal load. Under the same normal load condition, the greater the angular displacement amplitude was, the lower the surface polarization resistance was. Combined the analysis of morphology, it was found that the wear degree of surface would gradually increased with the increase of normal load and angular displacement amplitude. When  $F_n=10$  N and  $\theta=1.5^\circ$ , the joint effects of abrasive wear, adhesive wear and corrosion wear aggravated the damage of wear surface.

## ACKNOWLEDGEMENTS

This paper was supported by National Natural Science Foundation of China (No. 51705223) and University Natural Science Research Project of Jiangsu Province (No. 17KJB460005).

## References

1. D. Royhman, M. Patel, M.J. Runa, J.J. Jacobs, N.J. Hallab, M.A. Wimmer, *Tribol. Int.*, 91 (2015) 235.
2. A. Oladokun, M. Pettersson, M. Bryant, H. Engqvist, C. Persson, R. Hall, A. Neville, *Tribol.-Mater., Surf. & Interfaces*, 9 (2015) 165.
3. Y.J. Kao, C.N. Koch, T.M. Wright, D.E. Padgett, *J. Arthroplasty*, 31 (2016) 254.
4. Y. Zhou, M.X. Shen, Z.B. Cai, J.F. Peng, M.H. Zhu, *Wear*, 376 (2017) 670.

5. K. Kim, J. Geringer, *Wear*, 296 (2012) 497.
6. K. Kim, J. Geringer, J. Pellier, D.D. Macdonald, *Tribol. Int.*, 60 (2013) 10.
7. J. Geringer, J. Pellier, M.L. Taylor, D.D. Macdonald, *Tribol. Int.*, 68 (2013) 67.
8. Y. Liu, J.L. Gilbert, *Wear*, 390 (2017) 302.
9. D. Royhman, M. Patel, M.J. Runa, M.A. Wimmer, J.J. Jacobs, N.J. Hallab, M.T. Mathew, *J. Mech. Behav. Biomed. Mater.*, 62 (2016) 570.
10. C.T.D. Santos, C. Barbosa, M.J. Monteiro, I.C. Abud, I.M.V. Caminha, C.R.M. Roesler, *J. Mech. Behav. Biomed. Mater.*, 62 (2016) 71.
11. A. Panagiotidou, T. Cobb, J. Meswania, J. Skinner, A. Hart, F. Haddad, G. Blunn, *J. Orthop. Res.*, 4 (2017) 1.
12. J.S. Kawalec, S.A. Brown, J.H. Payer, K. Merritt, *J. Biomed. Mater. Res. A* 29 (1995) 867.
13. M. Viceconti, O. Ruggeri, A. Toni, A. Giunti, *J. Biomed. Mater. Res.*, 30 (1996) 181.
14. V. Swaminathan, J.L. Gilbert, *Biomaterials*, 33 (2012) 5487.
15. V. Swaminathan, J.L. Gilbert, *J. Biomed. Mater. Res. A*, 101 (2013) 2602.
16. D.J. Hall, R. Pourzal, H.J. Lundberg, M.T. Mathew, J.J. Jacobs, R.M. Urban, *J. Biomed. Mater. Res. B*, 8 (2017) 1.
17. M. Baxmann, S.Y. Jauch, C. Schilling, W. Blömer, T.M. Grupp, M.M. Morlock, *Med. Eng. Phys.* 35 (2013) 676.
18. K. Chen, D.K. Zhang, G.F. Zhang, T.Q. Hao, S.R. Ge, *Mater. Design* 56 (2014) 914.
19. F.E. Donaldson, J.C. Coburn, K.L. Siegel, *J. Biomech.*, 47 (2014) 1634.
20. J.H. Yi, X.Z. Lin, Z.B. Cai, M.X. Shen, L.P. He, M.H. Zhu, *Funct. Mater.*, 7 (2012) 919.
21. M.T. Mathew, M.J. Runa, M. Laurent, J.J. Jacobs, L.A. Rocha, M.A. Wimmer, *Wear*, 271 (2017) 1210.
22. J. Zhang, F.A. Moslehy, S.L. Rice, *Wear*, 149 (1991) 1.
23. J. Zhang, F.A. Moslehy, S.L. Rice, *Wear*, 149 (1991) 13.
24. S.Q. Wang, D.K. Zhang, N.N. Hu, J.L. Zhang, *Rsc Adv.*, 6 (2016) 66087.
25. Z.B. Cai, S.S. Gao, M.H. Zhu, X.Z. Lin, J. Liu, H.Y. Yu, *Wear*, 270 (2011) 230.
26. Z.B. Cai, G.A., Zhang, Y.K. Zhu, M.X. Shen, L.P. Wang, P.H. Zhu, *Tribol. Int.*, 59 (2013) 312.

© 2018 The Authors. Published by ESG ([www.electrochemsci.org](http://www.electrochemsci.org)). This article is an open access article distributed under the terms and conditions of the Creative Commons Attribution license (<http://creativecommons.org/licenses/by/4.0/>).